DOI: 10.1021/ma901882g

Macromolecules
ARTICLE

Influence of Crystal Polymorphism on the Three-Phase Structure and on the Thermal Properties of Isotactic Poly(1-butene)

Maria Laura Di Lorenzo,*,† Maria Cristina Righetti,‡ and Bernhard Wunderlich§,∥

†*Istituto di Chimica e Tecnologia dei Polimeri (CNR), c/o Comprensorio Olivetti, Via Campi Flegrei, 34, 80078 Pozzuoli (NA), Italy,* ‡*Istituto per i Processi Chimico-Fisici (CNR), Area della Ricerca, Via G. Moruzzi, 1, 56124 Pisa, Italy,* §*Department of Chemistry, The University of Tennessee, Knoxville, Tennessee, and* ∥ *Rensselaer Polytechnic Institute, Troy, New York*

Received August 24, 2009; Revised Manuscript Received October 12, 2009

ABSTRACT: The influence of crystal polymorphism on the three-phase structure of isotactic poly(1-butene) (PB-1) is discussed. Crystallization of PB-1 from the melt yields the tetragonal phase, known as form II. Upon storage, it spontaneously transforms to the trigonal form I. The chain motion within the crystalline parts varies strongly with the crystal structure and affects the coupled amorphous parts. The form II−form I solid−solid transformation is accompanied by a change in the thermal properties that involves all parts of the three-phase structure. The increased density and thermal stability of the crystals cause a higher rigidity of the coupled amorphous phases. In form I PB-1, the mobile amorphous phase (MAF) has a reduced heat capacity step at the glass-transition temperature that occurs at a slightly broadened temperature. The RAF is coupled more strongly to the rigid form I crystals and relaxes at higher temperatures compared with the polymer containing modification II crystals, which are conformationally disordered. Both polymorphs display only little reversibility of the melting process. It is almost negligible in form I PB-1 and more conspicuous in the form II crystals. The different behavior arises from the varied recrystallization kinetics, which is limited in extent for the trigonal polymorph.

Introduction

Isotactic poly(1-butene) (PB-1) is a polyolefin with a complex polymorphism. It can develop up to five crystal modifications when subjected to various thermal and mechanical histories.[1−3] The most common and widely studied crystalline structures are known as form I and form II. Form II is a tetragonal crystal modification packed as an 11/3 helix and is kinetically favored when the polymer is crystallized by cooling of the unstrained melt under atmospheric pressure. This crystal structure is metastable and upon storage spontaneously transforms into the twinned trigonal form I. The transformation is completed after about 10 days of storage at room temperature but takes longer if the polymer is annealed at higher temperature or stored at lower temperature.[4,5]

Despite thorough investigations of the kinetics of the form II−form I transformation, its mechanism is not fully understood. It is known that it occurs via nucleation at crystal sites that are locally under stress and results in beneficial materials properties, especially in terms of an improvement of mechanical performance, including higher hardness, stiffness, and strength.[3,6,7] These effects are caused neither by an increased crystallinity of the material because the crystal fraction does not change during the polymorphic transition nor by variation in crystal morphology.[8] Few details are known of the impact of this solid−solid phase transition on the thermal properties of PB-1. The main effect is a shift of the melting temperature by about 10−15 °C when the form II crystals are transformed into form I. Additionally, the two modifications have very different melting enthalpies, with heats of fusion equal to 62 ± 3 and 141 ± 10 J/g for forms II and I, respectively.[9]

*Corresponding author. E-mail: dilorenzo@ictp.cnr.it. Tel: +39-081-8675059. Fax: +39-081-8675230.

In the first paper of this series, a detailed analysis of the three-phase structure of isotactic PB-1 was presented.[10] Similar to many other semicrystalline polymers, PB-1 has two different types of amorphous fractions, characterized by different degrees of decoupling with the crystal phase. Besides the mobile amorphous phase (MAF), made of the chain segments that start relaxing at the glass transition (T_g) of the bulk-amorphous phase, and the crystal phase, a third fraction of nanosized dimensions, the rigid amorphous fraction (RAF), was introduced.[11,12] The RAF arises from partially crystallized macromolecules, which remain strongly coupled when crossing the phase boundaries and have a separate, higher glass-transition temperature than the MAF.

The relative amounts of the three phases in PB-1 depend on crystallization conditions. Fast crystallization conditions lead to low crystallinity and high RAF amounts. The RAF of PB-1 starts to vitrify only after completion of crystallization and is fully mobilized at temperatures > 50 °C. This was analyzed for the just-crystallized polymer in the tetragonal modification, but no details were provided in ref 10 of the kinetics of devitrification on the RAF coupled to crystals in the form I modification. This is described in the present contribution.

Additionally, in this article, a thorough discussion of the influence of crystal polymorphism on the thermal properties of isotactic PB-1 is presented. Main analyses are conducted by quasi-isothermal temperature-modulated calorimetry (TMDSC), which is at present the only experimental technique that can provide quantitative data on the detailed melting process of polymers. Such data on fusion are needed to gain insight into the complex nanophase structure of semicrystalline polymers to understand fully the processes related to the formation and evolution of the various phases that have been, at the moment, clarified only in part. The coupling between the crystal and amorphous fractions,

 Published on Web 10/30/2009

probed for a number of semicrystalline polymers, is shown for the first time to be largely affected by crystal polymorphism. In isotactic PB-1, the transition from the tetragonal to the trigonal modification imparts larger constraints on the amorphous material. The results of these investigations not only advance overall understanding of forms I and II and of their transition but are ultimately also expected to provide a direct link between the thermal and mechanical properties and the molecular structure and mobility of semicrystalline polymers. In the past, it was shown that the RAF and MAF as the interconnecting phases between the microphase crystals determine the overall mechanical properties of a semicrystalline sample.[13] It is thus of importance for the understanding of isotactic PB-1 to show for the first time that polymorphism can affect the glass transition of the RAF.

Experimental Part

Material. Isotactic PB-1 of melt flow rate equal to 0.4 g/10 min (190 °C/2.16 kg) was kindly provided by Basell Polyolefins. The material is a commercial PB-1 grade used for extrusion into pipe for potable hot and cold water distribution applications. It contains some nucleating agents, which are added to accelerate the form II−form I phase transformation.

Before analyses, the sample chips were compression-molded with a Carver Laboratory Press at a temperature of 160 °C for 5 min without any applied pressure to allow complete melting. After this period, a pressure of ~50 bar was applied for an additional 5 min; then, the compression-molded sheet was cooled to room temperature with cold water circulating in the plates of the press.

Calorimetry. Standard DSC (St-DSC) and temperature-modulated DSC (TMDSC) measurements were conducted with a Mettler DSC 822^e calorimeter (Mettler-Toledo). Dry nitrogen was used as purge gas at a rate of 30 mL/min. Cooling was accomplished with the liquid-nitrogen accessory for the Mettler DSC 822^e. The temperature of the calorimeter was calibrated with the onset of the transition peaks for indium, naphthalene, and cyclohexane. The heat flow rate was initially calibrated with the heat of fusion of indium and then refined with a baseline run of two empty aluminum pans and a calibration run with sapphire as a standard.[14]

To set the structure for the analysis of thermal properties, each PB-1 specimen was heated from 25 to 160 °C at a rate of 20 °C/min, melted at 160 °C for 10 min to erase previous thermal history, and then cooled at a rate of either 0.5 or 30 °C/min. As mentioned in the Introduction, PB-1 crystals grow in modification II upon cooling from the melt. These metastable crystals slowly transform into the more stable form I during storage at room temperature. For this reason, some PB-1 samples were immediately heated after cooling using linear ramps or temperature-modulated programs; other samples were, instead, maintained at room temperature for a time sufficient to ensure completion of the form II−form I transformation before being subjected to thermal analysis.

St-DSC measurements were conducted at a scanning rate of 20 °C/min from −60 to 160 °C. The TMDSC program was designed using the Star^e software of Mettler-Toledo. Nonisothermal TMDSC data were gained using a sawtooth oscillation with a temperature amplitude of 0.2 °C, an underlining heating rate of 1 °C/min, and modulation periods of 60 s. The quasi-isothermal program involved a modulation of 0.2 °C about the base temperature T_o, a period of 60 s, and stepwise temperature increments of 5 °C after 16 min at each T_o. The final 8 min at T_o were used for data evaluations. Extended-time quasi-isothermal analyses of a duration of 6 h were conducted at selected T_o temperatures. After completion of the extended-time quasi-isothermal experiments, the material was heated from T_o until complete melting at a linear scanning rate of 1 °C/min.

From TMDSC measurements, the reversing specific heat capacity ($c_{p,rev}$) was derived from the ratio of the amplitudes

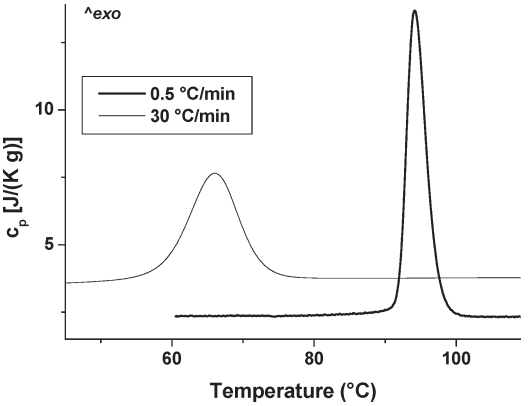

Figure 1. Specific heat capacity of PB-1 during cooling from the melt at the indicated rates. The curves are shifted along the y axis by 1.5 J/(K g) for clarity of presentation.

of modulated heat flow rate ($A_{\Phi,n}$) and temperature ($A_{T,n}$), both approximated with Fourier series[15]

$$c_{p,\mathrm{rev}}(\omega,n,t) = \frac{A_{\Phi,n}(t)}{A_{T,n}(t)}\frac{K(\omega,n,t)}{mn\omega} \quad (1)$$

where t is the time, n is the order of the harmonic, ω is the base modulation frequency ($\omega = 2\pi/p$), m is the mass of the sample, and $K(n,\omega,t)$ is the frequency-dependent calibration factor. The reversing specific heat capacity data reported in this contribution were obtained from the first harmonics of the Fourier series.

It needs to be underlined that some slight differences for samples subjected to similar thermal histories appear in the shapes of the plots presented here and in the previous article of this series;[10] these differences simply arise from the diverse resolution of the instrumentation.

Results and Initial Discussion

Isotactic PB-1 was crystallized from the melt using two constant cooling rates, 0.5 and 30 °C/min. With the used DSC, controlled cooling rates higher than 30 °C/min are difficult to achieve because of instrumental limitations, and this restricts the temperature range where isothermal crystallization after cooling from the melt can be performed. Therefore, nonisothermal crystallization at selected controlled cooling rates was preferred because this procedure allows a higher variation of crystallization conditions.[16] The temperature range where crystallization takes places during cooling at 0.5 and 30 °C/min is illustrated in Figure 1. When PB-1 is crystallized at 0.5 °C/min, the phase transition starts at 99 °C and appears to be completed around 91 °C, covering a time range of 16 min and a temperature interval of 8 °C. Cooling at 30 °C/min allows crystallization to be completed in a much shorter time, less than 1 min from the beginning of growth of the first crystals, which occurs at 78 °C, until complete impingement at 54 °C. For both cooling rates used, PB-1 develops a spherulitic morphology, as shown in Figure 2, that presents the optical micrographs of PB-1 crystals after cooling from the melt. As expected, lower cooling rates lead to reduced nucleation density and larger dimensions of the spherulites. In both cases, nucleation is heterogeneous because homogeneous nucleation in PB-1 occurs at undercoolings higher than 140 °C, that is, at temperatures much lower than those displayed in the Figure.[17]

Figure 3 presents the experimental specific heat capacity (c_p) of isotactic PB-1 after cooling from the melt at 30 °C/min, measured by St-DSC. On the same plot, TMDSC data obtained at the underlying heating rate of 1 °C/min and under quasi-isothermal conditions at steps of 5 °C (Q-Iso) are illustrated. These data are

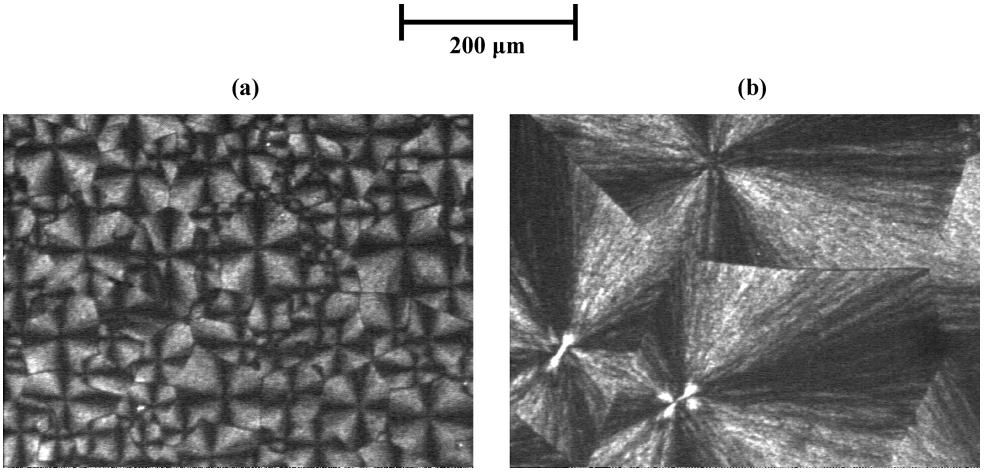

Figure 2. Optical micrographs (crossed polars) of PB-1 after crystallization from the melt at various cooling rates: (a) 30 and (b) 0.5 °C/min.

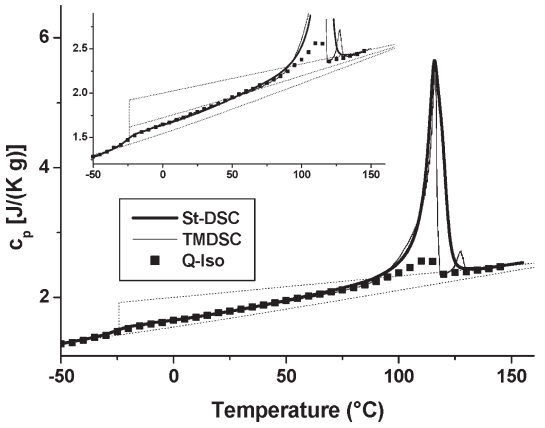

Figure 3. Specific heat capacity of PB-1 analyzed immediately after crystallization from the melt at 30 °C/min (form II). The thick solid line is the total heat capacity by St-DSC, the thin line is the reversing specific heat capacity measured by TMDSC, the solid squares represent the reversing heat capacity after 16 min of modulation at each T_o, and the dotted lines are the solid and liquid specific heat capacities, as taken from the ATHAS Data Bank.[18] The insert in the upper left corner is an enlargement of the plot in the baseline c_p area, showing also the c_p baseline calculated from the two-phase model.

compared in Figure 3 with thermodynamic c_p values of fully solid and liquid PB-1, as taken from the ATHAS Data Bank.[18] The insert in the upper left corner of Figure 3 shows an enlargement of the plots in proximity of the baseline c_p values. The total c_p data reveal a heat capacity step centered around −26 °C, caused by the glass transition (T_g) of the MAF, followed by a continue increase in the experimental heat capacity that remains below the baseline curve of liquid PB-1 until the onset of fusion. A main melting peak, due to fusion of PB-1 crystals in form II, is centered at 116 °C. The crystal fraction (w_C) was derived from the St-DSC curve using 62 J/g as the thermodynamic heat of fusion of form II crystals.[9,10] This yields a crystallinity of $w_C = 0.59$ for PB-1 crystallized from the melt at 30 °C/min. Comparison of the heat capacity step at the glass transition with the Δc_p step of fully amorphous PB-1, taken from the ATHAS Data Bank,[18] provides a mobile amorphous content $w_A = 0.24$. This results in a three-phase structure, with a RAF $w_{RA} = 0.17$. The phase composition is summarized in Table 1, which also shows the three-phase content of PB-1 subjected to varied thermal histories, discussed below.

For isotactic PB-1 crystallized from the melt at 30 °C/min and immediately analyzed (form II), the quasi-isothermal TMDSC plot at steps of 5 °C reveals a small amount of reversibility of the

Table 1. Three-Phase Composition of Isotactic PB-1 in Dependence of Thermal History

	w_A	w_C	w_{RA}
30 °C/min: form I	0.18	0.58	0.24
30 °C/min: form II	0.24	0.59	0.17
0.5 °C/min: form I	0.13_5	0.65	0.21_5
0.5 °C/min: form II	0.19	0.66	0.15

fusion of PB-1 crystals of form II. In the TMDSC curve gained with a nonzero underlying heating rate, a second, smaller apparent endotherm appears around ∼130 °C, probably caused by a minor fraction of PB-1 crystals of form I that have transformed from the metastable form II during the cooling from the melt and the slow TMDSC heating, as also noted in ref 10; however, such TMDSC data are often not quantitative,[19] and hence this small peak is not further discussed. The St-DSC and the two TMDSC curves are shown in Figure 3 to overlap from low temperatures, below the glass transition of the mobile amorphous fraction, up to ∼90 °C, close to the onset of the main melting peak, where the three plots intersect the baseline curve of fully liquid PB-1. The two-phase c_p curve is crossed at ∼50 °C, where full mobilization of the RAF of PB-1 takes place, as detailed in ref 10.

The thermal analysis of PB-1 with form I crystals is exhibited in Figure 4, which presents the St-DSC and TMDSC data of the sample cooled at 30 °C/min from the melt and maintained at room temperature for a time sufficient to complete the solid−solid transformation to the trigonal modification. Completion of the transition is probed by the St-DSC plot of Figure 4, which displays a single endotherm peaked at 128 °C, typical of modification I, and no evidence of the low melting peak expected for modification II, seen in Figure 3. Integration of the fusion endotherm and comparison with the thermodynamic heat of fusion of form I of 141 J/g[9,10] provides a crystal fraction $w_C = 0.58$. The minor difference with the value calculated for the sample with a predominant modification II structure is within the experimental error and confirms that no variation in overall crystallinity occurs when the form II crystals transform into form I, as has been reported in the literature.[6−9] A crystal fraction of $w_C = 0.58$ implies that the overall portion of the chains that are amorphous is equal to 0.42. The heat capacity step at the glass transition, which is centered at −25 °C, is smaller than that computed for a mobile amorphous fraction equal to 0.42, as better evidenced in the insert in the upper left corner of Figure 4, revealing that a considerable rigid amorphous nanophase fraction is present in PB-1 after the crystals have all transformed into modification I. The mobile amorphous fraction amounts

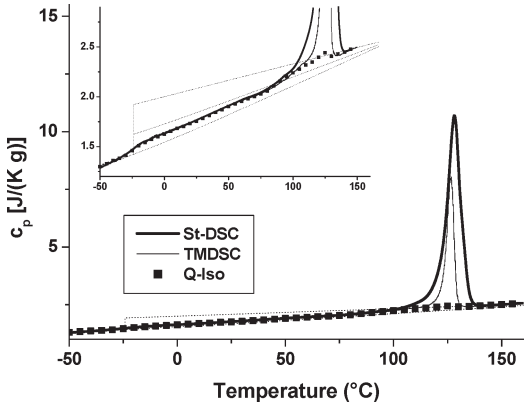

Figure 4. Specific heat capacity of PB-1 after crystallization from the melt at 30 °C/min and storage at room temperature (form I). The thick solid line is the total heat capacity by St-DSC, the thin line is the reversing specific heat capacity measured by TMDSC, the solid squares represent the reversing heat capacity after 16 min of modulation at each T_o, and the dotted lines are the solid and liquid specific heat capacities, as taken from the ATHAS Data Bank.[18] The insert in the upper left corner is an enlargement of the plot in the baseline c_p area, showing also the c_p baseline calculated from the two-phase model.

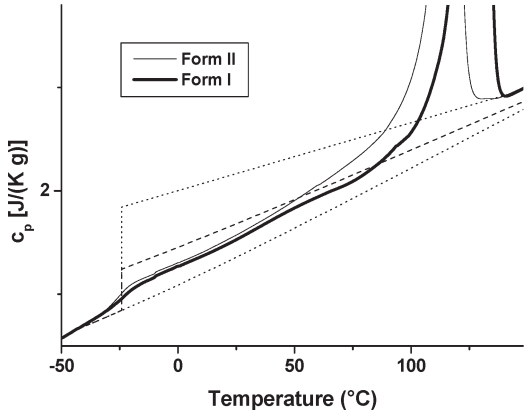

Figure 5. Specific heat capacity of PB-1 after crystallization from the melt at 30 °C/min. The thin solid line refers to PB-1 analyzed immediately after crystallization (form II), and the thick solid line refers to PB-1 stored at room temperature after crystallization (form I). The dotted lines are the solid and liquid specific heat capacities, as taken from the ATHAS Data Bank,[18] and the dashed line is the c_p baseline calculated from the two-phase model.

to $w_A = 0.18$, which corresponds to a rigid amorphous content $w_{RA} = 0.24$.

A considerable increase in rigid amorphous portions took place upon the solid-state transformation, which is evidenced in Figure 5, which compares the St-DSC plots of PB-1 cooled at 30 °C/min, analyzed immediately after crystallization and after storage at room temperature. The lesser content of mobile amorphous chains in form I PB-1 corresponds to a larger fraction of strained amorphous segments coupled to the crystal phase. A decreased heat capacity step following the form II−form I transition was also noticed in ref 20 but neither quantified nor discussed in terms of three-phase structure.

Figure 4 also provides significant details of the thermal properties of the RAF of PB-1 in the presence of form I crystals as the two-phase baseline is crossed at temperatures much higher than that observed in the corresponding PB-1 sample with form II crystals, around 95 °C. A shallow exotherm appears from 65 to 90 °C, as seen in the insert of Figure 4. The three-heating modes give nearly identical c_p values up to 95 °C, excluding latent heat exchanges as possible increase in the experimental heat capacity

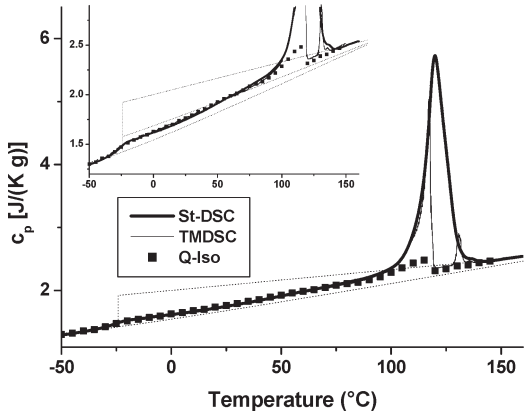

Figure 6. Specific heat capacity of PB-1 analyzed immediately after crystallization from the melt at 0.5 °C/min (form II). The thick solid line is the total heat capacity by St-DSC, the thin line is the reversing specific heat capacity measured by TMDSC, the solid squares represent the reversing heat capacity after 16 min of modulation at each T_o, and the dotted lines are the solid and liquid specific heat capacities, as taken from the ATHAS Data Bank.[18] The insert in the upper left corner is an enlargement of the plot in the baseline c_p area, showing also the c_p baseline calculated from the two-phase model.

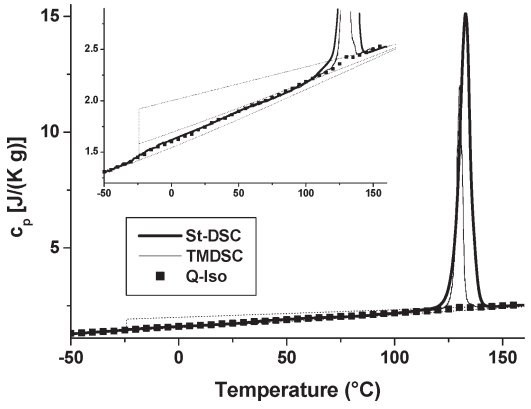

Figure 7. Specific heat capacity of PB-1 after crystallization from the melt at 0.5 °C/min and storage at room temperature (form I). The thick solid line is the total heat capacity by St-DSC, the thin line is the reversing specific heat capacity measured by TMDSC, the solid squares represent the reversing heat capacity after 16 min of modulation at each T_o, and the dotted lines are the solid and liquid specific heat capacities, as taken from the ATHAS Data Bank.[18] The insert in the upper left corner is an enlargement of the plot in the baseline c_p area, showing also the c_p baseline calculated from the two-phase model.

plots. This suggests that the RAF of PB-1 starts to mobilize at completion of T_g of the MAF and is fully relaxed around 95 °C. Above this temperature, the experimental c_p curves diverge because of the onset of fusion of PB-1 crystals. Some small reversibility is seen in the quasi-isothermal TMDSC plot of Figure 4 for PB-1 crystals in modification I, lower than the corresponding data of Figure 3 for the crystals in modification II, which is discussed below.

Figures 6 and 7 illustrate the St-DSC and TMDSC analyses of PB-1 after slow cooling from the melt at 0.5 °C/min with crystal modifications II and I, respectively. The reduced cooling rate imparts a different crystallization history, quantified in Figure 1, which produces corresponding variations in the thermal properties. The melting peak of form II PB-1 crystallized at 0.5 °C/min is centered at 120 °C, with a second, small peak around 136 °C due to fusion of a small fraction of crystals transformed to the trigonal modification I during cooling from the melt and the subsequent heating. Integration of the melting peak and analysis

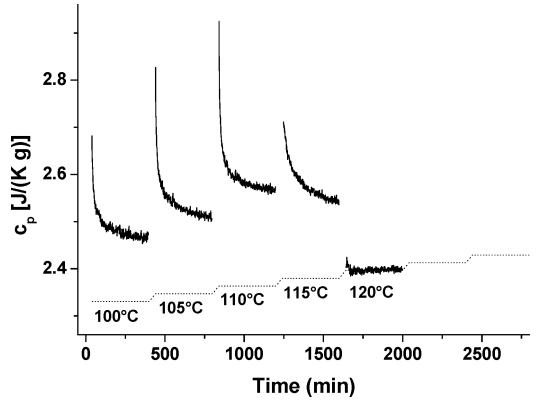

Figure 8. Time dependence of the reversing specific heat capacity of PB-1 during quasi-isothermal measurements at the indicated temperatures, analyzed immediately after crystallization from the melt at 30 °C/min (form II). The plots are shifted along the *x* axis for clarity of presentation. The data are from separate measurements and are collected in a single graph to compare the reversing c_p trends for different T_o values. The specific heat capacity of liquid PB-1, taken from the ATHAS data bank,[18] is shown as a dotted line for each T_o.

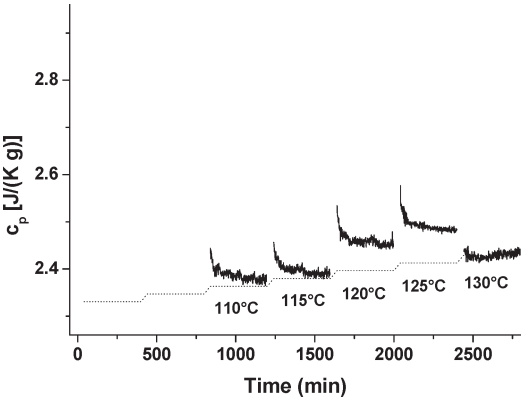

Figure 9. Time dependence of the reversing specific heat capacity of PB-1 during quasi-isothermal measurements at the indicated temperatures, analyzed after crystallization from the melt at 30 °C/min and storage at room temperature (form I). The plots are shifted along the *x* axis for clarity of presentation. The data are from separate measurements and are collected in a single graph to compare the reversing c_p trends for different T_o values. The specific heat capacity of liquid PB-1, taken from the ATHAS data bank,[18] is shown as a dotted line for each T_o.

of the heat capacity step at the glass transitions provide a crystal fraction $w_C = 0.66$, a MAF $w_A = 0.19$, and by difference a RAF $w_{RA} = 0.15$. As expected,[10] the slow crystallization conditions attained at low cooling rate from the melt favor the formation of a higher level of crystallinity and of a lower amount of RAF, compared with the cooling at 30 °C/min. Similar to the plots shown in Figure 3, the St-DSC and the TMDSC data agree closely from below the glass transition of the MAF up to the onset of the main melting peak, where the experimental data cross the heat capacity line of pure liquid PB-1.

The St-DSC and TMDSC data presented in Figure 7 are used to calculate the composition of the three-phase structure of PB-1 cooled from the melt at 0.5 °C/min and stored at room temperature for a time sufficient to complete the form II-form I transformation. This thermal history provides a crystal fraction $w_C = 0.65$, a MAF $w_A = 0.13_5$, and a RAF $w_{RA} = 0.21_5$. Similar to the polymer cooled at 30 °C/min, the solid−solid transformation implies no significant variation of the amount of crystalline material and a noteworthy modification in the mobility of the amorphous material, a decrease in the mobile amorphous content, and a corresponding increase in the RAF. As also shown by the data in Figure 4, the three thermal analysis plots of Figure 7 closely agree from low temperatures up to 105 °C, the onset of irreversible melting, where both the St-DSC and the two TMDSC curves cross the two-phase c_p baseline, as shown in the insert of Figure 7. The heat capacity line of the pure liquid is reached by St-DSC at 120 °C.

The TMDSC analyses of PB-1 as a function of time are presented in Figures 8 and 9, which illustrate the variation of reversing c_p in the melting range after fast crystallization at 30 °C/min for PB-1 samples with form II and form I crystals, respectively. On the same plots, the heat capacities of fully liquid PB-1 at the indicated temperatures are also reported. Data were gained in separate quasi-isothermal experiments, each of a duration of 6 h. At all analyzed base temperatures, the apparent reversing heat capacity decreases with time until complete melting occurs, at $T_o = 120$ and 130 °C for PB-1 of form II and form I crystallites, respectively. The curves can be fitted with a double exponential decay equation of the form

$$c_p(t) = c_{p,\infty} + a_1 e^{-t/\tau_1} + a_2 e^{-t/\tau_2} \quad (2)$$

where $c_{p,\infty}$ is the reversing c_p when extrapolated to infinite time, a_1 and a_2 are the pre-exponential factors, and τ_1 and τ_2 are the characteristic relaxation times. Results of the fit of experimental data with eq 2 are given in Table 2.

Table 2. Parameters of Double-Exponential Decays of Isotactic Poly(1-butene) during Quasi-Isothermal Modulations, According to the Equation: $c_p(t) = c_{p,\infty} + a_1 e^{-t/\tau_1} + a_2 e^{-t/\tau_2}$

Form I: Crystallized at 30 °C/min					
temp. Q-iso (°C)	$c_{p,\infty}$ (I)	a_1 (I)	τ_1 (I)	a_2 (I)	τ_2 (I)
110	2.37	0.042	11	0.030	210
115	2.38	0.041	19	0.024	210
120	2.45	0.056	18	0.019	290
125	2.48	0.043	19	0.026	230
Form II: Crystallized at 30 °C/min					
temp. Q-iso (°C)	$c_{p,\infty}$ (II)	a_1 (II)	τ_1 (II)	a_2 (II)	τ_2 (II)
100	2.47	0.12	8.5	0.073	91
105	2.51	0.18	8.1	0.095	110
110	2.57	0.21	6.7	0.098	74
115	2.53	0.096	21	0.11	139

The extrapolations to infinite time result in higher apparent heat capacities than expected not only for the corresponding semicrystalline samples but also for pure liquid PB-1, revealing the presence of a truly reversible latent heat contribution to the heat capacity. Both the pre-exponential factor and the relaxation times differ in magnitude upon variation of the crystal structure. Higher pre-exponential factors and lower relaxation times are quantified in Table 2 for PB-1 with crystals in modification II. This leads to larger values of the experimental reversing c_p extrapolated to infinite times for the polymer containing form II crystals, compared with form I crystals, at all analyzed temperatures. The prolonged modulation at $T_o = 115$ °C of PB-1 in form II gives a different kinetics of crystal reorganization than at lower temperatures with increased relaxation times.

St-DSC analyses were conducted after the long-time modulations. All traces reveal a single melting endotherm, indicating no change of the crystal modification during the prolonged annealing. From the St-DSC plots, the fusion peaks and the crystal fraction were estimated, and the values are given in Figures 10 and 11. Exposure at high temperatures results in a small increase in the melting point, revealing the increased thermal stability of the crystals caused by the prolonged annealing for both modifications I and II. A larger increment is noted after the quasi-isothermal modulation of modification II at 115 °C that may be

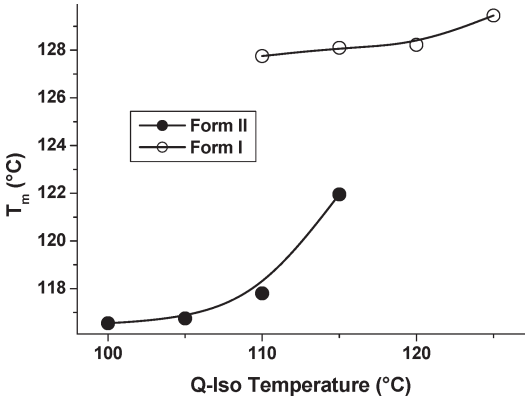

Figure 10. Melting peak temperatures (T_m) of PB-1 crystallized at 30 °C/min after 6 h of quasi-isothermal modulation, measured at a scanning rate of 1 °C/min.

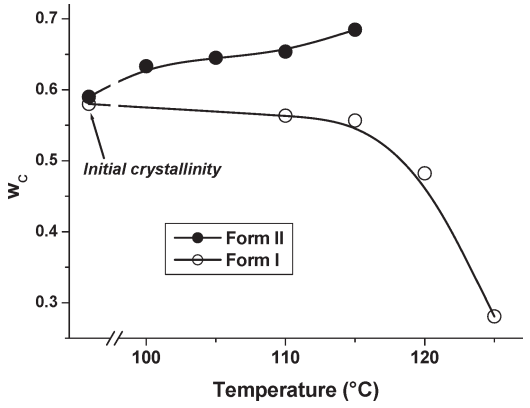

Figure 11. Crystal fraction (w_C) of PB-1 crystallized at 30 °C/min after 6 h of quasi-isothermal modulation. The initial crystallinity is also reported.

linked to the varied reversing c_p decay kinetics. Additionally, the overall crystal fraction is differently affected in the two crystal modifications by the long-time modulation at high temperature. The crystallinity in isotactic PB-1 of form II increases after the prolonged annealing, which becomes more pronounced with the increase in the base temperature of modulation. The opposite trend is seen for form I, where the overall crystallinity decreases, as shown in Figure 11.

Final Discussion

Three-Phase Structure. Isotactic PB-1, similar to many other semicrystalline polymers,[12] has a three-phase structure made of crystalline and mobile-amorphous microphases and additional rigid amorphous nanophases.[12,13] In ref 10, a quantitative analysis of the three-phase composition in dependence of thermal history was detailed for PB-1 samples containing form II crystals. The relative amounts of the phases are mostly affected by the crystallization kinetics. Faster crystallization rates favor the formation of lower crystallinity and larger amounts of RAF.[10] This information is now confirmed by the thermal analyses detailed in this study and summarized in Table 1 not only for the polymer containing form II crystals but also after completion of the solid−solid transformation from the metastable tetragonal modification to the stable trigonal structure. The most relevant data arising from Table 1 concern the variation of mobility of the amorphous phases after completion of the solid−solid transformation, indicated by the increase in the RAF, which produces a reduced step in c_p at the glass transition of the MAF. The interpretation of these observations is to be discussed next.

The rigid amorphous nanophases are most likely located at the folded-chain interface between bulk amorphous and crystal, and hence the two crystal phases are expected to affect the mobility of the coupled amorphous parts differently. The chain dynamics of isotactic PB-1 depends on the crystalline modification, as was proven by nuclear magnetic resonance.[21−24] At temperatures below T_g of the bulk-amorphous phase, rotation of the methyl group is quite similar in all polymorphs, despite larger differences in crystal density. This equivalence arises from the weaker intramolecular interactions in the 3/1 helix of form I compared with the 11/3 helix of form II, which compensate the denser intermolecular packing.[21] At temperatures above T_g, however, the chain motions within the crystalline parts vary with structure.[21] In form I, the polymer chains are almost rigid in the crystalline domains up to 87 °C.[23] Higher temperatures were not investigated because of the closeness to the onset of melting. Conversely, large-amplitude motion occurs within the backbone of the crystals of form II. The main chains adopt locally distributed conformations with transitions among them.[22−24] The conformational disorder along the helix axis, coupled to the preservation of the periodical order in the transverse plane, makes modification II a conformational disordered (condis) crystal. The conformational disordered arrangement implies segmental motions of the chains within the lattice, which reduces the strain on the amorphous parts of the molecules coupled to the crystal, resulting in a lesser amount of RAF in semicrystalline PB-1 with crystals of form II.

The presence or absence of differently ordered structures alone does not necessarily cause a variation in the RAF. A specific mobility, as just described for the PB-1 is necessary for such changes. An example of little or no influence of crystal structure on the RAF was observed for isotactic polypropylene (PP), which displays a polymorphic behavior, including a modification with intermediate crystalline order, a condis crystal, as discussed first in ref 25. Slow crystallization from the melt yields the monoclinic α lattice, which may be accompanied by some amount of the trigonal β modification, which grows at high undercoolings or in the presence of specific nucleants. Additional crystal modifications have been proven for isotactic PP, including the condis structure, which develops upon rapid cooling. It has a conformational disordered array similar to form II of PB-1. By using different crystallization pathways, followed by annealing, it is possible to produce PP samples that exclusively contain either the monoclinic form or the condis crystal with the same crystallinity. For the same crystallinity, the RAF does not vary with the regularity of the crystal phase. The same amount of RAF was proven in PP with either monoclinic or mesophase structure for a broad range of samples with the same crystallinity.[26] The different crystallinities and crystal structures of PP were achieved by imparting very different thermal histories, involving crystallization from the melt at different rates, followed by variable subsequent annealing. This is different from the PB-1, detailed in the present research, where the two polymorphs with the same crystallinity were obtained by cooling at the same rate from the melt. It is only with the subsequent annealing at room temperature that the metastable condis lattice of PB-1 was transformed into the more ordered form I. Additionally, the transitions from the metastable condis to the stable crystal structure are quite different in the two polyolefins. In PB-1, the solid−solid transformation needs nucleation at crystal sites and a major reassembly of the

chains, whereas no nucleation is required in PP because the transition involves no change in helix type.[1,3] Moreover, in PB-1, the transition from tetragonal to trigonal modification takes place at temperatures below the upper end of the glass transition of the condis phase, whereas in PP, the solid−solid transformation starts as soon as the T_g of the mesophase is reached.

The form II−form I transformation of PB-1 is connected with densification of the chains within the crystal phase. The 11/3 helices of modification II are loosely packed, with a crystal density $\rho_{II} = 0.907$ g/cm^3, slightly higher than that of the amorphous state, $\rho_a = 0.868$ g/cm^3, whereas the chain packing in the 3/1 helical conformation of modification I corresponds to a crystal phase with much higher density, $\rho_I = 0.95$ g/cm^3.[3] In other words, PB-1 crystals reduce their specific volume by ∼4% at completion of the solid−solid transformation. The reduction in volume of the crystal phase can increase the strain to the coupled amorphous chain portions at the crystal−amorphous interface, which results in a higher amount of RAF with an additionally reduced mobility and thus a higher T_g than the RAF of form II PB-1.

Physical aging by densification of the amorphous phases was associated with the formation of a constrained amorphous fraction and additional mobility of the remaining MAF.[27] This can be excluded as a possible cause of the reduced overall mobility of the amorphous fraction associated with the form II−form I phase transformation in PB-1. After long time annealing at room temperature, the quickly cooled and the slowly cooled samples both showed a possible exotherm in the inserts in Figures 4 and 7 in the glass-transition regions of the RAF rather than an endotherm that is normally connected with physical aging of amorphous phases. The structure analysis of quenched isotactic PP aged for varying times at room temperature similarly showed densification of the crystallinity without variation of the overall crystallinity. This also should not be considered to be an aging, a term usually only applied to the annealing of amorphous solids.

Influence of Crystal Polymorphism on the Temperature-Dependence of the Three-Phase Structure. The different mobility of the two polymorphs of isotactic PB-1 largely affects their thermal analysis. It was noted above that St-DSC and TMDSC curves of PB-1 containing either form I or form II crystals coincide over a wide temperature range, from below the glass-transition temperature up to the onset of melting. The different crystallization history, with crystals slowly grown at high temperatures or quickly developed upon rapid cooling from the melt, only affects the onset of melting and the reversing nature of the melting peaks. The almost-perfect match of the plots also includes the quasi-isothermal analysis, where irreversible processes are excluded and the reversible c_p is approached. The St-DSC and the TMDSC curves start to diverge around 90−100 °C, depending on the crystallization history and the crystal lattice. At this temperature, the experimental heat capacity reaches the baseline c_p level of pure liquid PB-1 (form II) or crosses the baseline c_p curve computed on the basis of a two-phase structure, where all amorphous material is mobilized (form I). The specific volume of both modifications I and II linearly increases up to melting,[28] which makes the occurrence of a glass transition within the crystal phase above 100 °C unlikely to be possible contribution to the reversible heat capacity before melting, as recently probed for a number of other semicrystalline polymers, including aliphatic polyamides and polyoxides.[29,30]

The matching of the DSC traces seen in Figures 3, 4, 6, and 7 implies that no irreversible melting takes place in PB-1 form II up to 60−70 °C and form I up to 90−100 °C. In ref 10, it was already shown that a broad glass transition of the RAF of form II takes places from above T_g of the MAF up to ∼50 °C, where all amorphous chain segments are fully mobilized. Above 50 °C, weak frequency-dependence of the reversing heat capacity reveals some exchange of latent heat, which, however, becomes fully reversible after 8 min of quasi-isothermal modulation, as seen in Figures 3 and 6. It is likely that the large angle motions within the condis crystal allow a continuous gain in mobility of the chains until a liquid-like mobility is reached around 90−95 °C, corresponding to the glass transition of the condis phase.

The case of PB-1 containing rigid form I crystals is different. Both total and reversing c_p continuously increase from the upper end of the glass transition of the MAF up to ∼100 °C, where the experimental data intersect the two-phase baseline, with the only exception of a weak and broad exotherm that extends from 65 to 90 °C in the St-DSC plot, caused by irreversible latent heat exchanges. This allows us to assign the raise in reversing c_p to mobilization of the RAF, which completes its glass transition only at ∼100 °C. The weak and broad exotherm in the St-DSC plots of form I PB-1 that takes place before the onset of melting can be ascribed to processes involving either the crystal phase or the RAF. For a number of semicrystalline polymers, it was shown that the large coupling between the crystal and amorphous parts affects the reorganization of the crystals. These reorganizations can occur only if the amorphous segment chains in proximity of the crystal/melt interface have sufficient mobility, which can be achieved upon release of the strain of the amorphous chain segments coupled to the just-melted crystals.[12,13,31,32] Some ordering at the crystal surface made possible by the just-mobilized coupled RAF segments may account for this small release of latent heat. The shallow exotherm may also reveal some secondary crystallization occurring during the heating scan. Secondary crystallization takes place in geometrically restricted areas in which the melt undergoes larger constraints. Partial release of these constraints due to mobilization of the RAF may favor further development of crystals, confirming a link between secondary crystallization and RAF vitrification.[33−35] Secondary crystallization in form II PB-1 might be masked by the increase in mobility in the condis crystals. A stress release of the rigid amorphous segments may be another possible cause of the shallow thermal event before the onset of melting of form I PB-1 crystals. This may be linked to the weak exotherm that takes place upon completion of T_g of the MAF of form II PB-1, which is detailed in ref 10.

The varied glass transition of the RAF of PB-1-containing crystals in modifications I and II can be explained by taking into account the different degrees of coupling between the RAF chain segments with the crystalline parts. The backbone motions originating from the chains in the amorphous domains are transmitted to the helices in the crystalline areas and vice versa. The long-range order of the helices largely hinders motions within the trigonal crystals, which induces tight constraints in the coupled amorphous parts. Conversely, the conformational disorder of form II helices permits large angle motions of the chain backbone above T_g, which results in a decreased strain imparted to the amorphous segments coupled to the condis crystals. As a consequence, the RAF segments can reach full mobility at lower temperature compared with the polymer with form I crystals.

Time-Dependent Melting. The quasi-isothermal mode of TMDSC allows us to extend the experimental analysis until all irreversible processes are completed so that one can quantify remaining reversible processes and separate them

from irreversible events like crystal rearrangements, annealing, and recrystallization. A number of reversible and irreversible contributions to the apparent heat capacity have thus been identified. Known reversible contributions include the vibrational heat capacity, the conformational changes that produce an increase beyond the vibrational heat capacity, and the reversible melting. Typical irreversible processes comprise crystal perfection, secondary crystallization, and primary crystallization and melting.

The predominant irreversible character of melting of both the analyzed polymorphs of isotactic PB-1 can be quantified from the data shown in Figures 3, 4, 6, and 7 by comparison of the St-DSC and the quasi-isothermal TMDSC plots outside of the melting region. The large supercooling seen with the data of Figure 1 suggests little or no overlap between cooling and heating curves, permitting no truly reversible melting, as can be seen for normal paraffins with less than ~75 chain atoms.[12]

To discuss the influence of irreversible contributions to the apparent reversing heat capacity of PB-1 in the melting range, the thermal analysis data gained after the long-time quasi-isothermal experiments, shown in Figures 10 and 11, need to be taken into account. The increase in the melting point after 6 h of treatment at high temperatures reveals the occurrence of annealing and crystal perfection, which leads to lamellae with increased thickness, lesser concentration of nonequilibrium defects, or both, with limited or no secondary crystallization having taken place.

The structural rearrangements in PB-1 during the solid−solid transformation involve both crystal and amorphous chain portions, as detailed above. At the temperatures of extended quasi-isothermal analyses, however, all amorphous chain portions in PB-1 are above their respective T_g, which excludes a possible influence of the RAF on reversible melting, as reported in the literature for other semicrystalline polymers.[12,13,32,36]

Recrystallization during the quasi-isothermal experiments, aided by molecular nucleation, appears to be the key reason for the small amount of reversible melting of PB-1 polymorphs. As remarked above, crystallization of isotactic PB-1 from the melt yields the metastable tetragonal form II. Modification I does not develop upon direct crystallization from the melt but only upon slow transformation of form II. Chain conformations in these two crystal structures are different in their sequence of close-to trans and gauche dihedral angles along the main chain.[37] In each heating segment during the extended-time quasi-isothermal experiments, a portion of ordered molecules within the crystals become disordered (melt). In the case in which the initial crystals are in the tetragonal modification, recrystallization can take place, provided that the requisite molecular nucleation is satisfied. Conversely, recrystallization in the same crystal structure for the trigonal PB-1 is kinetically less favored. Epitaxial growth of PB-1 from the melt on specific substrates can lead to form I′, which has the same chain packing as form I but a much lower melting temperature, below the range of the prolonged quasi-isothermal experiments.[38] This explains the different reversibility of the melting process of the two analyzed polymorphs of isotactic PB-1, sizable for form II and almost negligible for form I. In form II, PB-1 recrystallization of the just-melted crystals takes place when the modulation reverses the temperature change, whereas in form I samples, partial melting is not followed by recrystallization of the chain into the same crystal lattice but may take place according to the tetragonal chain arrangement of modification II. For form II, PB-1 recrystallization at all analyzed temperatures is revealed by the increase in crystallinity after the quasi-isothermal experiments, quantified in Figure 11. Conversely, the crystal fraction of form I PB-1 slightly decays after 6 h of modulation at temperatures up to 115 °C and then rapidly decreases after exposure at $T_o \geq 120$ °C. At $T_o = 120$ °C, form II crystals are melted, as also seen in Figure 8, and no recrystallization in form II is possible, which results in a considerable decrease in crystallinity of PB-1 samples with initial crystals in the trigonal modification after the long quasi-isothermal experiments at 120 and 125 °C.

It needs to be underlined that the crystal fraction was computed on the basis of enthalpy of fusion of form I, considering that all crystals are in this modification. No lower melting peak was seen in the DSC traces measured immediately after the quasi-isothermal experiments, which, however, might be masked within the large melting endotherm of form I. If a portion of the crystals is in form II, then the overall crystallinity is obviously higher because of the much lower melting enthalpy of form II. This can explain the very slight decrease in the calculated crystallinity after the quasi-isothermal modulations up to 115 °C, which may be a slight increase if crystallinity were computed with the proper enthalpy of fusion for both fractions of crystal present in the sample. However, this approximation does not affect the overall discussion.

Conclusions

Quantitative St-DSC and TMDSC of the semicrystalline PB-1 have been used to evaluate the thermodynamics of its three-phase structure, which is globally metastable. The contributions from vibrational molecular motion to the heat capacity provide the baseline for the solid state of all three phases. Large-amplitude motion of the backbone chain affects a nanometer-sized space along and between the chains. It can be identified by the increase in c_p in the glass-transition temperature range. The lowest glass transition is that of the bulk-amorphous phase (MAF), which is centered at about −26 °C. Because the beginning of this glass transition does not change in temperature with crystallinity, but its end is moved to a higher temperature on partial crystallization, one can identify the amorphous phase volumes as microphases, coupled to the ordered phases. The other two phases have been identified as RAF nanophases with a glass transitions independent of and higher than that of the MAF. Crystal form II is a condis phase, and its coupling to the RAF nanophase causes a lower glass transition than the stable crystal phase of form I. A small fraction of reversibly melting crystals is observed and might involve in all cases the crystal form II. As in other macromolecules, the amount of reversible melting is larger for less well-crystallized samples.

The detailed phase structure analysis illustrated here for PB-1 shows that each linear macromolecule needs a full characterization to understand the structure−property correlations.[13] For the most flexible macromolecules, such as polyethylene, there is no separate RAF with an independent, higher glass-transition temperature; a two-phase structure describes the semicrystalline state.[39] For rigid macromolecules, such as poly(oxy-2,6-dimethyl-1,4-phenylene), there is no MAF, and again a two-phase structure is observed, but the only amorphous phase is the RAF. In this case, however, the glass transition of the RAF is higher than the melting temperature and determines the melting and annealing kinetics.[31] The here-analyzed PB-1 represents an intermediate macromolecule, which needs three phases for the description of the semicrystalline state, and in addition, the different crystal structures are connected to differently coupled RAF nanophases. This connection imparts varied thermal properties to the amorphous parts coupled to the different PB-1

polymorphs because the RAF coupled to tetragonal crystals attains full mobility at lower temperatures compared with the rigid amorphous portions coupled to trigonal crystals. This results not only from the increased density of the crystal phase attained upon the solid−solid transition but also from the varied mobility of the crystals coupled to the RAF, conformationally disordered in form II and more rigid in form I. In other words, the solid−solid transition from the tetragonal to the trigonal modification has implications not only on the arrangements on the chains within the crystal phase, as widely shown in the literature, but also on the amorphous chain portions coupled to the more or less ordered polymorphs.

Acknowledgment. We express our gratitude to Dr. Gilberto Moscardi of Basell Poleolefins for kindly providing the PB-1 sample.

References and Notes

(1) Wunderlich, B. *Macromolecular Physics: Crystal Structure, Morphology, Defects*; Academic Press: New York, 1973; Vol. *1*.
(2) Cojazzi, G.; Malta, V.; Celotti, G.; Zannetti, R. *Macromol. Chem.* **1976**, *177*, 915–926.
(3) Azzurri, F.; Flores, A.; Alfonso, G. C.; Baltá Calleja, F. J. *Macromolecules* **2002**, *35*, 9069–9073.
(4) Natta, G.; Corradini, P.; Bassi, I. W. *Nuovo Cimento* **1960**, *15*, 52–67.
(5) Azzurri, F.; Gómez, M. A.; Alfonso, G. C.; Ellis, G.; Marco, C. *J. Macromol. Sci., Phys.* **2004**, *B43*, 3177–3189.
(6) Luciani, L.; Seppälä, J.; Löfgren, B. *Prog. Polym. Sci.* **1988**, *13*, 37–62.
(7) Azzurri, F.; Flores, A.; Alfonso, G. C.; Sics, I.; Hsiao, B. S.; Baltá-Calleja, F. J. *Polymer* **2003**, *44*, 1641–1645.
(8) Rubin, I. D. *J. Polym. Sci.* **1964**, *B2*, 747–749.
(9) Alfonso, G. C.; Azzurri, F.; Castellano, M. *J. Therm. Anal. Calorim.* **2001**, *66*, 197–207.
(10) Di Lorenzo, M. L.; Righetti, M. C. *Polymer* **2008**, *49*, 1323–1331.
(11) Suzuki, H.; Grebowicz, J.; Wunderlich, B. *Makromol. Chem.* **1985**, *186*, 1109–1119.
(12) Wunderlich, B. *Prog. Polym. Sci.* **2003**, *28*, 383–450.
(13) Wunderlich, B. *Thermal Analysis of Plymeric Materials*; Springer: New York, 2005.
(14) Archer, D. G. *J. Phys. Chem. Ref. Data* **1993**, *22*, 1441–1453.
(15) Androsch, R.; Moon, I.; Kreitmeier, S.; Wunderlich, B. *Thermochim. Acta* **2000**, *357−358*, 267–278.
(16) Di Lorenzo, M. L.; Silvestre, C. *Prog. Polym. Sci.* **1999**, *24*, 917–950.
(17) Wunderlich, B. *Macromolecular Physics: Crystal Nucleation, Growth Annealing*; Academic Press: New York, 1976; Vol. *2*.
(18) *ATHAS Data Bank*; Pyda, M, Ed. http://athas.prz.rzeszow.pl/.
(19) Di Lorenzo, M. L.; Wunderlich, B. *Thermochim. Acta* **2003**, *405*, 255–268.
(20) Chau, K. W.; Yang, Y. C.; Geil, P. H. *J. Mater. Sci.* **1986**, *21*, 3002–3014.
(21) Maring, D.; Meurer, B.; Weill, G. *J. Polym. Sci., Part B: Polym. Phys.* **1995**, *33*, 1235–1247.
(22) Beckham, W. H.; Schmidt-Rohr, K.; Spiess, W. H. *ACS. Symp. Ser.* **1995**, *598*, 242–253.
(23) Maring, D.; Wilhelm, M.; Spiess, H. W.; Meurer, B.; Weill, G. *J. Polym. Sci., Part B: Polym. Phys.* **2000**, *38*, 2611–2624.
(24) Miyoshi, T.; Hayashi, S.; Imashiro, F.; Kaito, A. *Macromolecules* **2002**, *35*, 6060–6063.
(25) Wunderlich, B.; Grebowicz, J. *Adv. Polym. Sci.* **1984**, *60/61*, 1–59.
(26) Zia, Q.; Mileva, D.; Androsch, R. *Macromolecules* **2008**, *41*, 8095–8102.
(27) Agarwal, M. K.; Schultz, J. M. *Polym. Eng. Sci.* **1981**, *21*, 776–781.
(28) Starkweather, H. W., Jr.; Jones, G. A. *J. Polym. Sci., Part B: Polym. Phys.* **1986**, *24*, 1509–1514.
(29) Qiu, W.; Habenschuss, A.; Wunderlich, B.; *Polymer* **2007**, *48* 1641−1650.
(30) Qiu, W.; Pyda, M.; Nowak-Pyda, E.; Habenschuss, A.; Wunderlich, B. *Macromolecules* **2005**, *38*, 8454–8464.
(31) Pak, J.; Pyda, M.; Wunderlich, B. *Macromolecules* **2003**, *36*, 495–499.
(32) Di Lorenzo, M. L. *Polymer* **2009**, *50*, 578–584.
(33) Xu, H.; Ince, B. S.; Cebe, P. *J Polym. Sci., Part B: Polym. Phys.* **2003**, *41*, 3026–3036.
(34) Righetti, M. C.; Tombari, E.; Angiuli, M.; Di Lorenzo, M. L. *Thermochim. Acta* **2007**, *462*, 15–24.
(35) Righetti, M. C.; Tombari, E.; Di Lorenzo, M. L. *Eur. Polym. J.* **2008**, *44*, 2659–2667.
(36) Righetti, M. C.; Di Lorenzo, M. L.; Angiuli, M.; Tombari, E. *Macromolecules* **2004**, *37*, 9027–9033.
(37) Corradini, P.; Guerra, G. *Adv. Polym. Sci.* **1991**, *100*, 183–217.
(38) Kopp, S.; Wittmann, J. C.; Lotz, B. *Polymer* **1994**, *35*, 916–924.
(39) Wunderlich, B. *Macromolecular Physics: Crystal Melting*; Academic Press: New York, 1980; Vol. *3*.